

# Proposal for THz generation by an Unbiased and antenna-coupled CW Terahertz Photomixer

M. J. Mohammad-Zamani and M. K. Moravvej-Farshi  
Faculty of Electrical and Computer Engineering,  
Advanced Devices Simulation Lab (ADSL),  
Tarbiat Modares University,  
Tehran, Iran  
[m.mohammadzamani@modares.ac.ir](mailto:m.mohammadzamani@modares.ac.ir), &  
[Farshi\\_k@modares.ac.ir](mailto:Farshi_k@modares.ac.ir)

M.Neshat  
School of Electrical and Computer Engineering,  
University of Tehran  
Tehran, Iran  
[mneshat@ut.ac.ir](mailto:mneshat@ut.ac.ir)

**Abstract**— We introduce an array of new antenna-coupled and unbiased terahertz photomixer. Unlike previous structures, this emitter does not require any external bias voltage. In this work, we show that an array of asymmetric (bi-metallic) MSM structures, whose unit cell (pitch) is made of a pair of dissimilar Schottky contacts on LTG-GaAs can act as bias free CW THz photomixer emitters. For photocarrier acceleration it rather makes use of the built-in electrostatic Schottky contact field formed at the electrode-photoconductor interface. Moreover, we demonstrate 5  $\mu$ W of THz power radiation in the 0.5 THz can be achieved by using a dipole antenna integrated with the proposed unbiased photomixer. A hybrid numerical simulation method is used to model and analyze this phenomenon.

**Keywords**- Carrier transport; photomixer; terahertz; bias-free

## I. INTRODUCTION

The biased THz photomixers have been widely used as potentially compact, low cost, low power consuming, coherent, room temperature, and highly tunable CW THz sources in recent years [1, 2]. In this regard, the idea of using a bias free THz emitter can be a gateway to overcome the disadvantages appeared in the rival structures. A bias free THz photomixer is a potentially attractive THz radiation source for biomedical applications. As have been already demonstrated experimentally [3] and theoretically, [4, 5], unlike the large aperture (LA) emitters [6], for efficient acceleration of photogenerated carriers, do not require DC biases in the kV range. Moreover, unlike the scalable microstructured photoconductive emitters [7, 8], a bias free THz photomixer does not suffer from the short circuit defects that likely occur in the gap between two adjacent fingers in interdigitated emitters, ruining the operation of the entire device. Besides, the bimetallic bias free THz emitters have an advantage over those bias free sources based on lateral photo-Dember method [9,10]. The former emitters, unlike the latter sources, do not suffer from limitation in choice of photoconductors with distinct electrons and holes mobilities and the complexity in fabrication of suitable electrodes [10]. For CW mode, to the best of our knowledge, there is no detailed study of coupled-antenna bias-free photomixer in the literature.

In this paper, we will focus on the study and simulation of an antenna-coupled and unbiased CW THz photomixer with bi-metallic electrodes. The device structure and its operation principle are described in Section II, the simulation results and discussion follows in Section III, with the conclusion in Section IV.

## II. DEVICES STRUCTURE AND SIMULATION MODELS

In the proposed bi-metallic structure, the emitter does not need any external bias field for photocarrier acceleration as the inherent Schottky fields present at the bimetallic/semiconductor interface are used for the charge-carrier acceleration.

The new emitter uses grating structures made of two different metals that are formed on a photoconductive substrate. CW THz wave generation can be triggered by optical excitation of the structure through combination of the output of two single mode lasers with different center frequencies that falls in the THz range. The key feature enabling terahertz generation is based on the application of two different metal materials with different work functions. There is a net lateral field at bimetallic gratings resulting from the Schottky-field difference between both metals used. Otherwise a single metal generates exactly equal and opposing internal fields that results in the generation of equal photocurrents in the opposite directions. Opposing currents generate THz fields that cancel out through destructive interference. It should be emphasized that in this new approach the generation mechanism of photocurrent is different from that in photo-Dember effect. Here, the acceleration of photo-carriers within the internal electrostatic fields at the metal-semiconductor interface or the so-called space charge regions produces photocurrent. Therefore, the photocurrent generated due to Schottky fields is orders of magnitude higher than the current produced due to the diffusion process as in photo-Dember effect.

Also, the active area in the new unbiased and antenna-coupled emitter can be scaled to square-mm sizes in order to handle high optical powers, and a short-cut of a single gap does not affect the functionality of the whole device as does in biased scalable emitters.

### A. Devices Structure

In this section, the proposed photomixer structure is described. Fig. 1 illustrates a cross sectional view of the building block of the model bias-free photomixer made of an asymmetric MSM structure that can also serve as the unit cell of a periodic array of the modeled bias-free THz photomixer emitters. Each emitter pitch, with lateral dimension of  $A$ , consists of a pair of dissimilar metallic strips ( $M_1$  and  $M_2$ ) that are deposited in parallel with lateral spacing  $s$ , on top of a 1- $\mu\text{m}$  thick layer of LTG-GaAs to make a pair of dissimilar Schottky barriers  $\Phi_{B1} > \Phi_{B2}$ . In such a structure, a metallic planar antenna is also placed on the fast photoconductive material LTG-GaAs that is connected to dissimilar metallic strips ( $M_1$  and  $M_2$ ). On the other hand, the photomixer array is coupled to a planar antenna and thereby, radiates the generated THz power. A photomixer array is used when a photoconductive antenna array is desired [11] or in scalable THz emitters.

The device is illuminated from the top by two optical plane waves whose frequency difference falls in THz band. Total incident optical power density is  $0.4 \text{ mW}/\mu\text{m}^2$  and the beat frequency is 0.5 THz. In order to model the array, a periodic boundary condition is applied on the two sides along the  $x$ -direction of the simulation domain. Physical parameters of the modeled photomixer with LTG-GaAs substrate are given in Table. I . We have already shown, elsewhere [5], that only certain choices of materials for  $M_1$  and  $M_2$  that provide permissible pairs of  $s$  and  $\Delta\Phi_B$  values, for which the strength of the electric field maxima are below that of the critical DC breakdown electric field for LTG-GaAs [12]– i.e.,  $E_{\text{max}} \leq 50 \text{ V}/\mu\text{m}$ – beyond which the device will operate properly. The constituents’ geometrical dimensions and values of the physical parameters used in our simulations can be found in Table I.

### B. Modeling of Optical Carrier Generation and Carrier Transport

Electron and hole pairs are generated by photon absorption when the device is illuminated by two optical waves. In order to model the optical generation, we initially obtain the intensity distribution from the time-averaged Poynting vector. Due to the difference of input optical frequencies, total optical generation rate is modulated by the difference frequency. The time-dependent optical generation rate is used in a carrier

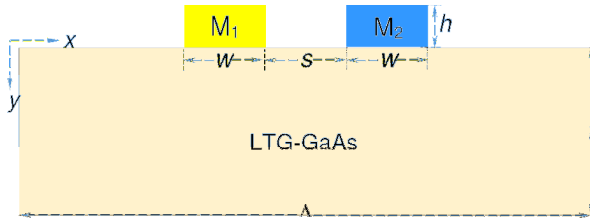


Fig. 1. Cross sectional view of the unit cell of a periodic array of the bias-free THz photomixer emitters, each consisting of an interconnected pair of dissimilar Schottky contacts on LTG-GaAs layer. The array pitch size is  $A$ .

Table I. Geometrical and physical parameters of the modeled LTG-GaAs photomixer

Symbol	Parameter	Value	Unit
$h$	Contact thickness	200	nm
$s$	Lateral terminals spacing	180	nm
$t$	Substrate thickness	1	$\mu\text{m}$
$w$	Contact width	200	nm
$A$	Pitch size	1400	nm
$\lambda_0$	Laser center wavelength	800	nm
$\Delta f$	Input signals frequency difference	0.5	THz
$I_0$	Total optical power density	400	$\mu\text{W}/\mu\text{m}^2$
$\alpha$	Absorption coefficient	1	$\mu\text{m}^{-1}$
$\tau_{n0}$	Low field electron life time	0.1	ps
$\tau_{p0}$	Low field hole life time	0.4	ps
$\mu_{n0}$	Low field electron mobility	400	$\text{cm}^2/\text{V}\cdot\text{s}$
$\mu_{p0}$	Low field hole mobility	100	$\text{cm}^2/\text{V}\cdot\text{s}$
$\epsilon_r$	Relative permittivity	13.8	–
$A_n$	Effective electron Richardson coefficient	6.2875	$\text{A}/\text{cm}^2\cdot\text{T}^2$
$A_p$	Effective hole Richardson coefficient	105.2	$\text{A}/\text{cm}^2\cdot\text{T}^2$
$\Phi_{B1}$	Schottky Barrier height of Metal 1	1.11	eV
$\Phi_{B2}$	Schottky Barrier height of Metal 2	0.8	eV
$T$	Temperature	300	K

transport model that is to be numerically solved in the time domain to obtain the THz current and field.

We used the drift–diffusion model to calculate the generated THz photocurrent inside the photoconductor layer. A set of drift–diffusion equations in the time domain includes the Poisson’s equation, the continuity equations for electrons and holes, and the current relations for electrons and holes. In order to solve the set of carrier transport equations, finite element method (FEM) is used. In modeling of carrier transport process, carrier generation/recombination is an important process in this device. For the net recombination rate in the drift–diffusion model, the Shockley–Read–Hall (SRH) and Auger processes are considered [13]. In addition, we need to consider the appropriate boundary conditions to solve the set of equations properly. In this regard, along the outer (non-contact) edges of devices, homogeneous (reflecting) Neumann boundary conditions are imposed so that current only flows out of the device through the contacts. In the absence of surface charge along such edges, the normal electric field component becomes zero [14]. At the interface of the metal and semiconductor, the boundary condition for the Schottky contact is based largely on the approach introduced by Crowell and Sze [15]. This approach is derived from the boundary condition of a thermionic recombination velocity ( $V_R$ ) near the metal–semiconductor interface. The contact acts as a source or sink for carriers and consequently it can be treated as a surface recombination mechanism. The recombination velocities ( $V_n$  and  $V_p$ ) are determined by assuming that the dominant source of current across the junction is thermionic emission [14–15].

### III. RESULTS AND DISCUSSION

The numerical results obtained for the distribution of the time-averaged carrier photogeneration rate inside the LTG–GaAs is shown in Fig. 2. The carrier photo-generation rate is not uniform, and the effect of scattering from the metallic edges can be observed in the LTG–GaAs layer.

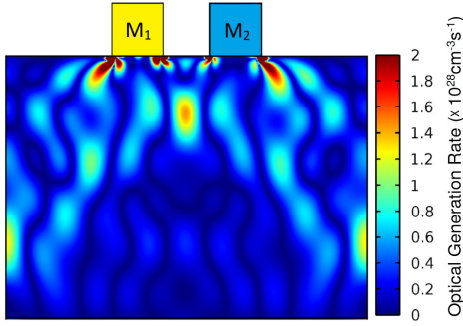


Fig. 2. Time-averaged carrier photo-generation inside the LTG-GaAs layer of photomixer at 0.5 THz

The electric potential is computed by solving the continuity equations coupled to the Poisson's equation. Calculated electrostatic potential and electric field for the photomixer are shown in Fig. 3 for a point located in the gap at the interface of the LTG-GaAs and air.

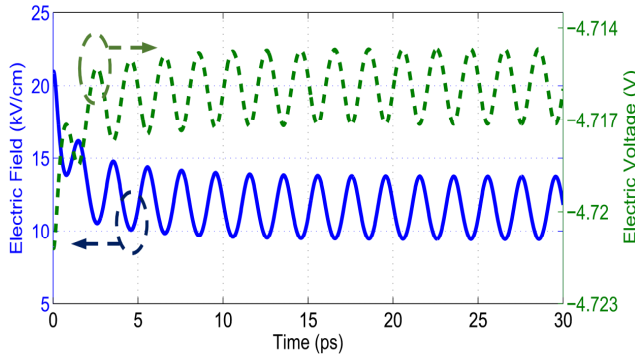


Fig. 3. (a) Electric field (bottom) and potential (top) versus time at 0.5 THz.

By solving the drift-diffusion equations, the current densities are obtained. According to the Schottky contacts, the total current density can be found by  $\mathbf{J} = \mathbf{J}_{th,n} + \mathbf{J}_{th,p}$ , where  $\mathbf{J}_{th,n}$  and  $\mathbf{J}_{th,p}$  are the electron and hole thermionic current density, respectively [14]. The total generated THz photo-current has two components: DC and AC (or THz). Various components of THz photocurrent versus time are plotted in Fig. 4.

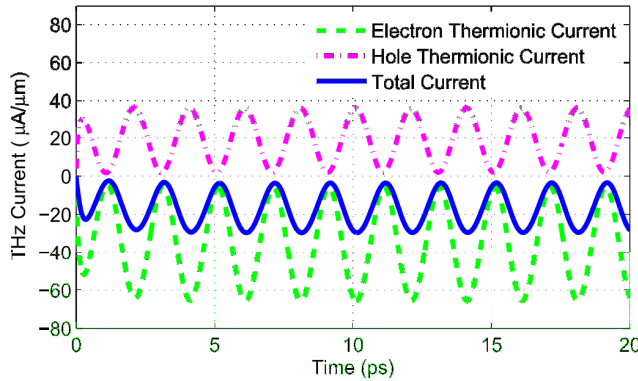


Fig. 4. Various components of THz photo-current at  $M_2$  electrode versus time at 0.5 THz

Fig. 5 shows a time snapshot of the local electric fields ( $E_x$  and  $E_y$ ) distributions inside the LTG-GaAs layer of the photomixer. The  $x$ - and  $y$ -components of the electrostatic electric field ( $E_x$  and  $E_y$ ) distributions in the active area can be obtained by taking the gradient of the corresponding CB diagram, with respect to  $x$ - and  $y$ -directions. As can be observed from these figures, strengths of  $E_x$  and  $E_y$  are significant within the narrow regions about the contacts edges and become negligible outside these regions. It should be noted that their directions also indicate the direction of their current components. The asymmetry observed in this electric field ( $E_x$  and  $E_y$ ) diagrams for this structure with dissimilar electrodes provide potential differences between the electrodes with value of 310 meV. When the device is under appropriate illuminations, the  $\Delta\Phi_B$  in each case can cause the photogenerated carriers within the space charge region to flow in and out through the dissimilar contacts.

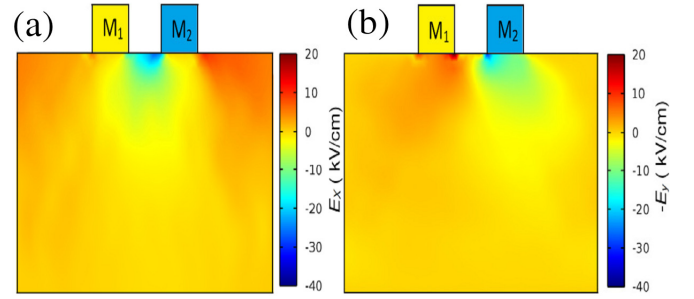


Fig. 5. Snapshots of the components of the local electric fields: (a)  $E_x$  and (b)  $-E_y$ , within the LTG-GaAs substrate, at a given moment.

Fig. 6 shows a time snapshot of the 2D distributions of the lateral and transverse components of the total local current density ( $J_{phx}$  and  $J_{phy}$ ) within the LTG-GaAs of the same emitter. Negative and positive values of the total local current components at any given point shown in Figs. 6 (a) and 6 (b), are determined by the direction of the electric field components (Figs. 5 (a) and 5 (b)).

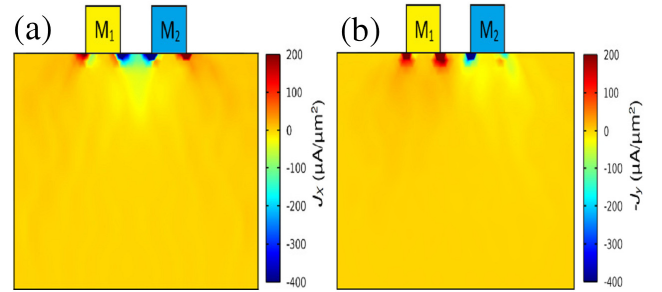


Fig. 6. Snapshots of the components of the local current densities: (a)  $J_{phx}$  and (b)  $-J_{phy}$ , within the LTG-GaAs substrate, at a given moment.

Finally, we have investigated the possible output power level for the proposed structure. For this, full-wave electromagnetic solvers based on method of moment or finite-element method (FEM) can be used for numerical simulation of the output THz antenna structure to determine the antenna input impedance as a function of frequency. Moreover, The

THz current obtained in the active area in the LTG-GaAs are used as a current source in the antenna feed point. For broadband applications, it is of interest to have uniform radiated THz power over a wide range of frequencies. For this purpose, broadband antennas such as a bow-tie antenna are integrated with the photomixer device [1], [16-18]. On the other hand, resonance antennas such as a dipole antenna provide higher radiation resistance at the resonance frequency as compared to broadband antennas, and consequently, increase the THz power radiations around the resonance. In the following, the THz power obtained from a center-fed dipole antenna (300  $\mu\text{m}$  long) and a bow-tie antenna integrated with the proposed photomixer device is investigated.

Calculating the generated THz photocurrent and obtaining radiation resistance, the ideal radiated THz power of the photoconductive antennas can be calculated as [19]:

$$P_{\text{THz}} = \frac{1}{2} R_{\text{Antenna}} I_{\text{THz}}^2 \quad (1)$$

In this regard, we have obtained the THz photocurrent in the proposed photomixer for different beat frequencies, first. The numerical simulation results for the amplitude of the THz photocurrent versus the beat frequency have shown in Fig. 7 (a). As expected, the THz photocurrent decreases at high frequencies.

By applying the (1) and using the results given in fig. 7 (a), we have calculated the THz radiation power from a 10- $\mu\text{m}$  wide (in z-direction) pitch photomixer emitter. Fig. 7 (b) compares the radiated power from the bow-tie and dipole antennas used as output antennas integrated with photomixer emitter. The behavior of plots is comparable to the results presented in [1],[20]. It should be noted that the curves plotted in the inset of Fig. 7 (b) depicts the radiation resistances of the bow-tie and dipole antennas (300  $\mu\text{m}$  long) that taken from [21] and used in the calculation of THz power according to (1). As can be observed in Fig. 7 (b), the radiated THz power is maximized near the resonant frequency (0.5 THz) of the dipole antenna so that 5  $\mu\text{W}$  of THz power radiation in the 0.5 THz can be achieved by using a dipole antenna integrated with the proposed unbiased photomixer. Using the broadband bow-tie antenna, the radiated THz power is more uniform for the whole range of frequencies rather than being maximized at a certain frequency. Obviously, if the radiation resistance of the broadband antenna has less variation over the range of frequencies, more uniform radiated THz power spectrum can be obtained although is still frequency dependent.

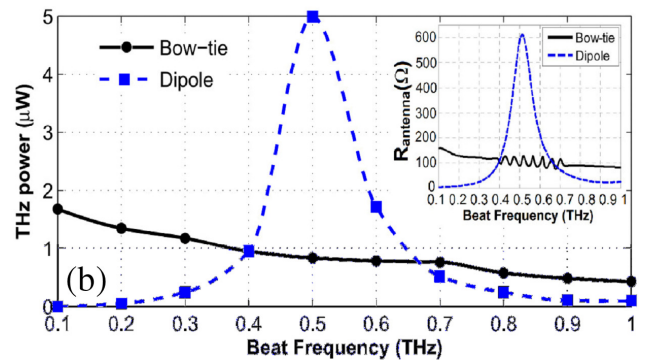
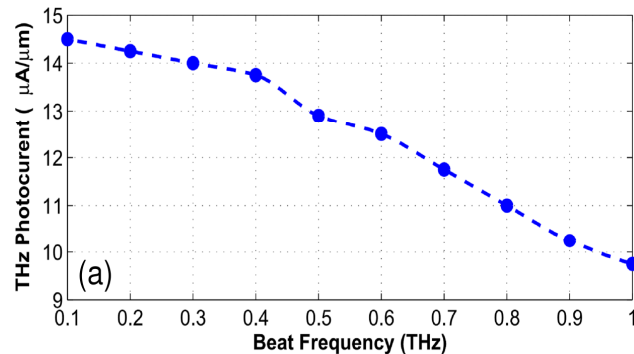


Fig. 7. The numerical simulation results for: (a) The Amplitude of THz photocurrent versus beat frequency, (b) The THz radiation output power from a 10- $\mu\text{m}$  wide (in z-direction) photomixer emitter versus beat frequency. The bow-tie and dipole antennas used as output antennas integrated with photomixer emitter. (the inset of Fig. 7 (b) depicts the radiation resistance of bow-tie and dipole antennas versus beat frequency that taken from [21]) .

#### IV. CONCLUSION

We studied a new generation of unbiased and antenna-coupled scalable CW THz photomixers. In this work, we have shown that an array of asymmetric (bi-metallic) MSM structures, whose unit cell (pitch) is made of a pair of dissimilar Schottky contacts on LTG-GaAs can act as bias free CW THz photomixer emitters. Our simulations confirm the possibility of CW photomixing and THz emission in an array of unbiased and coupled-antenna metallic electrodes due to photocarrier acceleration in the internal Schottky contacts, and despite the absence of any external bias voltage. Therefore, the emergence of this type of source can be a gateway to many applications, especially in medical applications such as endoscopic imaging where applying external voltage inside the body is not safe, and may cause serious health risks.

#### REFERENCES

- [1] I. S. Gregory et al., "Optimization of photomixers and antennas for continuous-wave THz emission," *IEEE J. Quantum Electron.*, vol. 41, no. 5, pp. 717–728, Sep./Oct. 2005.
- [2] M. C. Teich, "Field-theoretical treatment of photomixing," *Appl. Phys. Lett.*, vol. 14, no. 6, pp. 201–203, 1969.
- [3] M. Nagel, "Photoconductive structure e.g. radiation source, for optical generation of field signals in terahertz-frequency range in bio analysis, has metallic layers formed from locations and provided in direct contact with semiconductor material, European Patents Office, 2013, [DE102012010926 \(A1\)](https://patents.google.com/patent/DE102012010926/A1)
- [4] M. J. Mohammad-Zamani, M.K. Moravvej-Farshi, and M. Neshat, "Modeling and designing an unbiased CW terahertz photomixer emitters," in *Proceedings of the 3rd Conference on Millimeter Wave & Terahertz Technologies*, 30 Dec. 2014-1 Jan. 2015, Tehran, Iran. <http://dx.doi.org/10.1109/MMWaTT.2014.7057196>.
- [5] M. J. Mohammad-Zamani, M.K. Moravvej-Farshi, and M. Neshat, "Unbiased CW terahertz photomixer emitters with dis-similar Schottky barriers," *Opt. Exp.*, Vol. 23, No. 15, 19129, 2015.
- [6] J. T. Darrow, X.-C. Zhang, D. H. Auston, and J. D. Morse, "Saturation Properties of Large-Aperture Photoconducting Antennas," *IEEE J. Quantum Elec.*, vol. 28, no. 6, pp. 1607-1616, 1992.

- [7] S. Winnerl, "Scalable microstructured photoconductive terahertz emitters," *Journal of infrared, millimeter and terahertz waves*, Vol. 33, 2012, S. 431-454. - ISSN 1866-6892
- [8] A. Dreyhaupt, S. Winnerl, T. Dekorsy and M. Helm, "High-intensity terahertz radiation from a microstructured large-area photoconductor", *Appl. Phys. Lett.* 86, 121114 (2005)
- [9] G. Klatt et al., "Terahertz emission from lateral photo-Dember currents", *Optics Express*, Vol. 18, Issue 5, pp. 4939-4947 (2010)
- [10] V. Apostolopoulos and M. E. Barnes, "THz emitters based on the photo-Dember effect", *J. Phys. D: Appl. Phys.*, vol. 47, pp. 374002, 2014.
- [11] Erik Brundermann, Heinz-Wilhelm Hubers, Maurice FitzGerald Kimmitt, *Terahertz Techniques*, Springer, 2012.
- [12] E. R. Brown, "THz generation by photomixing in ultrafast photoconductors," *Int. J. High Speed Electron. Syst.*, vol. 13, no. 2, pp. 497-545, 2003.
- [13] M. Neshat, D. Saeedkia, L. Rezaee and S. Safavi-Naeini, "A Global Approach for Modeling and Analysis of Edge-Coupled Traveling-Wave Terahertz Photoconductive Sources," *IEEE Transactions on Microwave Theory & Techniques*, Vol. 58, No. 7, pp. 1952 - 1966, July 2010.
- [14] S. Selberherr, *Analysis and Simulation of Semiconductor Devices*. Wien, Austria: Springer-Verlag, 1984..
- [15] C.R. Crowell and S.M. Sze, "Current Transport in Metal-Semiconductor Barriers," *Solid State Electronics*, vol. 9, pp. 1035-1048, 1966.
- [16] E. R. Brown, K. A. McIntosh, K. B. Nichols, and C. L. Dennis, "Photomixing up to 3.8 THz in low-temperature-grown GaAs," *Appl. Phys. Lett.*, vol. 66, no. 3, pp. 285-287, 1995.
- [17] S. Verghese, K. A. McIntosh, and E. R. Brown, "Highly tunable fiber coupled photomixers with coherent THz output power," *IEEE Trans. Microw. Theory Techn.*, vol. 45, no. 8, pt. 2, pp. 1301-1309, Aug. 1997.
- [18] E. Peytavit, A. Beck, T. Akalin, J.-F. Lampin, F. Hindle, C. Yang, and G. Mouret, "Continuous terahertz-wave generation using a monolithically integrated horn antenna," *Appl. Phys. Lett.*, vol. 93, p. 111108, 2008
- [19] S. Preu, G. H. Dohler, S. M. Alzer, L. J. Wang, and A. C. Gossard, "Tunable, continuous-wave THz photomixer sources and applications," *J.MAppl. Phys.*, vol. 109, p. 061301, 2011.
- [20] S. Matsuura, M. Tani, and K. Sakai, "Generation of coherent THz radiation by photomixing in dipole photoconductive antennas," *Appl. Phys. Lett.*, vol. 70, no. 5, pp. 559-561, 1997.
- [21] M. Khabiri, M. Neshat and S. Safavi-Naeini, "Hybrid Computational Simulation and Study of Continuous Wave Terahertz Photomixers," *IEEE Tran. Terahz. Sci. Technol.* 2(6), 605-616 (2012).